

# Intermetallic compound layer formation in indium-based micro-bump array fabrication technology for IR detectors

Paweł Kozłowski<sup>1\*</sup>, Agata Jasik<sup>1</sup>, Adam Łaszcz<sup>1</sup>, Krzysztof Czuba<sup>1</sup>,  
Krzysztof Chmielewski<sup>1</sup>, Krzysztof Zdunek<sup>2</sup>

<sup>1</sup>Lukasiewicz Research Network – Institute of Microelectronics and Photonics, Al. Lotników 32/46, 02-668 Warsaw, Poland

<sup>2</sup>Warsaw University of Technology, Faculty of Materials Science and Engineering, ul. Wołoska 141, 02-507 Warsaw, Poland

## Article info

### Article history:

Received 12 Jul. 2023

Received in revised form 16 Oct. 2023

Accepted 30 Oct. 2023

Available on-line 15 Dec. 2023

### Keywords:

Indium micro-bump;  
under bump metallization;  
intermetallic alloy;  
focused ion beam;  
energy dispersive spectrometry.

## Abstract

This work reports on the investigation of homogeneity of the inside of indium micro-bumps/columns placed on Ti/Pt/Au under bump metallisation. This is very important for connection resistivity, long-time durability, and subsequent hybridisation process (e.g., die-bonding). Gold reacts with indium to form intermetallic alloys with different chemo-physical parameters than pure indium. The geometrical and structural parameters of intermetallic alloys were analysed based on transmission electron microscope images. Distribution of elements in the investigated samples was determined using the transmission electron microscope with energy dispersive spectroscopy method. A thickness of intermetallic alloy was 1.02  $\mu\text{m}$  and 1.67  $\mu\text{m}$  in non-annealed (A) and annealed (B) indium columns, respectively. The layered and column-like interior structure of alloys was observed for both samples, respectively, with twice bigger grains in sample B. The graded chemical composition of Au-In intermetallic alloy was detected for the non-annealed In columns in contrast to the constant composition of 40% of Au and 60% of In for the annealed sample B. The atomic distribution has a minor impact on the In column mechanical stability. A yield above 99% of an In column with a 25  $\mu\text{m}$  diameter and a 11  $\mu\text{m}$  height is possible for a uniform columnar structure of intermetallic alloy with a thickness of 1.67  $\mu\text{m}$ .

## 1. Introduction

Indium is widely used for electrical interconnections in various semiconductor devices due to its physicochemical properties. This is especially true for producing infrared (IR) photodetectors and focal plane arrays. A high flexibility, even at low temperatures, predisposes it as a material of choice for micro-connections in cooled devices [1–3], regardless of whether or not it is subjected to thermal cycling due to either cryogenic or thermoelectric cooling. Furthermore, it can reduce the stress resulting from different values of thermal expansion coefficients of the connected components [4, 5]. Nowadays, in IR detection applications, typical indium bumps have a diameter between 5  $\mu\text{m}$  and 20  $\mu\text{m}$ . Such short connections provide excellent electrical characteristics (e.g., smaller inductance), which is important

for operation at very high frequencies [6, 7]. The use of densely packed micro-meter-sized indium bumps significantly increases the signal-to-noise ratio of the device [8, 9]. Tomada *et al.* have estimated that the resistance of a single indium bump is about 2  $\Omega$  after flip-chip bonding [10]. The resistance is dependent on the structure and durability of the intermetallic alloy layer. In addition, the low melting point of indium (156 °C) and high plasticity guarantee no structural damage to both the detector and mount/readout electronics [11, 12]. Nevertheless, some problems in indium-based micro-bump array technology were identified. The mechanical stability of indium columns is one among them [13]. It impacts the yield and electrical properties of the connection between joined elements.

Our previous experiment showed that In columns have better adhesion to under bump metallisation (UBM) after annealing at 120 °C [14]. Increasing the temperature accelerates the process of AuIn<sub>2</sub> phase formation, which

\*Corresponding author at: [pawel.kozlowski@imif.lukasiewicz.gov.pl](mailto:pawel.kozlowski@imif.lukasiewicz.gov.pl)

leads to a strengthening of the bonding between the In column and the underlying Au layer. The obtained yield was above 99% for  $320 \times 256$  focal plane arrays. The issue of the uniformity of the intermetallic alloy layer and the optimal thickness of the Au layer for the ratio of the UBM layer to the diameter of In columns was left open. In this article, this problem has been clarified.

## 2. Experimental procedures

Indium columns were formed using thermal evaporation and a lift-off technique according to all technological procedures described in Ref. 14. Briefly, in a 200 nm thick SiO<sub>2</sub> passivation layer, 5 μm in diameter circular contact windows were opened for a UBM deposition. Then, a stack of 10 nm thick Ti, 20 nm thick Pt, and 300 nm thick Au was deposited. Next, indium was thermally evaporated in a Balzers 510 apparatus. The deposition rate was about 5 nm/min and the substrate was kept at about 10 °C during the process. Indium columns of about 21 μm in diameter and 11 μm high formed a  $320 \times 256$ -pixel array with a pixel pitch of 30 μm. To investigate intermetallic alloys between In columns and the Au layer from UBM, three cross-sections of the columns (three samples) were made using a focused ion beam (FIB) technique. The cross-sections of non-annealed (sample A) and annealed at 20 °C for 5 min in nitrogen atmosphere (sample B) indium columns were prepared without cooling during FIB preparation. The third cross-section was made for the annealed In column using a cooled FIB stage (sample C). The samples were prepared in a Helios NanoLab 600 FIB/scanning electron microscope (FIB/SEM) system, which uses liquid nitrogen as a coolant. The cooling process was carried out using a Kammrath & Weiss LN<sub>2</sub> Cryo Module installed in a FIB/SEM chamber. The samples were placed directly on the cooled stage; only the sides of the samples were glued to the plate with carbon tape. A cross-section of sample C was made at a temperature in the range from -70 °C to -50 °C. Without cooling, the temperature in the FIB/SEM system chamber is typically about 25 °C. SEM imaging was carried out at a temperature of about -50 °C. Transmission electron microscope (TEM) and energy dispersive spectrometry (EDS) were also used during cross-section investigations. The structures of indium-based micro-bumps were observed in an SEM at 20 kV of beam energy. All FIB processes leading to the fabrication of TEM lamellas were performed using an ion-beam energy of 30 kV and an ion-beam

current ranging from nanoamperes to picoamperes. Deposition of protective layers was not used during the fabrication of TEM lamellas in FIB. TEM observation and TEM/EDS analysis were performed at a beam energy of 200 kV.

## 3. Results

The yield of mechanically stable In columns on sample A was 50–60% while on samples B and C above 99%. The yield for sample A was dependent on the time elapsed since its fabrication. The cross-sections of In columns selected from the first row of the array were made for all investigated samples. SEM images of the cross-section of sample A with non-annealed In columns made without FIB stage cooling are shown in Fig. 1. The cross-section of In column selected for TEM analysis is presented in Fig. 1(b). Voids between an intermetallic compound and indium are visible in the lamella, Fig. 1(c), but much more clearly in Fig. 2(a), where the TEM image is presented. The width of the observed slit is in the range from 0.1 μm to 0.4 μm, depending on the measurement site. The intermetallic alloy is 1.22 μm thick at its thickest point. It can be seen that the intermetallic alloy contains three areas with different textures marked in Fig. 2(b): a solid layer close to the dielectric layer (1), a layer with small grains (2), and bigger grains (3). The diameter of the biggest grain with clearly defined boundaries in the area labelled as (3) reaches 600 nm. EDS was used to determine the composition of the intermetallic alloy. Both discrete measurements and EDS maps were taken. The former were performed in the three areas of the intermetallic alloys marked in Fig. 2(b). The EDS map is presented in Fig. 2(c). The material in point 1 probably contains 100% Au. The material in point 2 contains 61% Au and 39% In. The material in point 3 contains 40% Au and 60% In. The rest is also mainly silicon. The material above the voids is pure indium, while the layer above the SiO<sub>2</sub> is composed of pure gold. The EDS map shown in Fig. 2(c) confirms the presence of pure indium, a void, Au-In alloy with graded composition, and pure gold near the SiO<sub>2</sub> layer.

To increase the column yield and time-dependent stability, the In columns have been annealed in an N<sub>2</sub> atmosphere at 120 °C for 5 min. It resulted in a yield above 99%. The cross-section of sample B was also made without the FIB cooling stage. The results are presented in Fig. 3. Similarly to sample A, the cross-section revealed voids but smaller ones. The slit width is 0.2 μm on average [Fig. 3(a)].

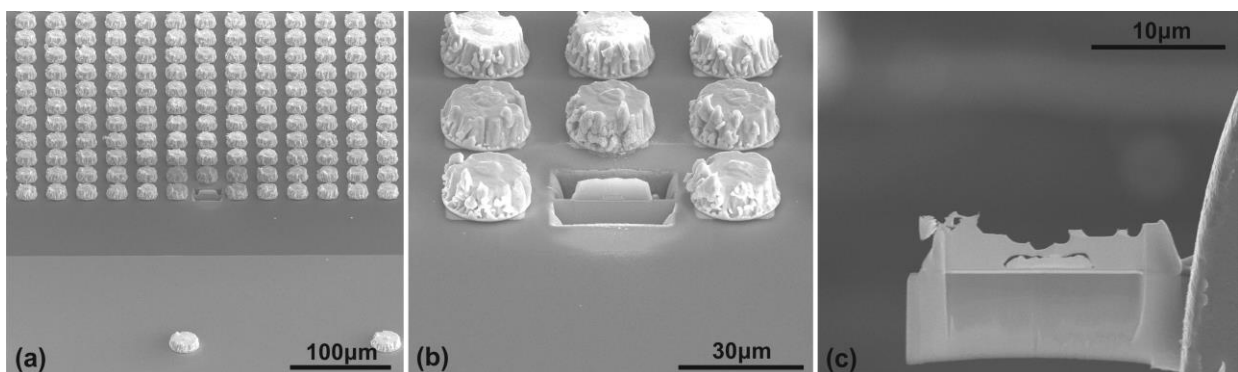


**Fig. 1.** SEM images of sample A: In columns (a), FIB cross-section made without cooling stage (b), lamella of In column prepared for TEM investigations (c).

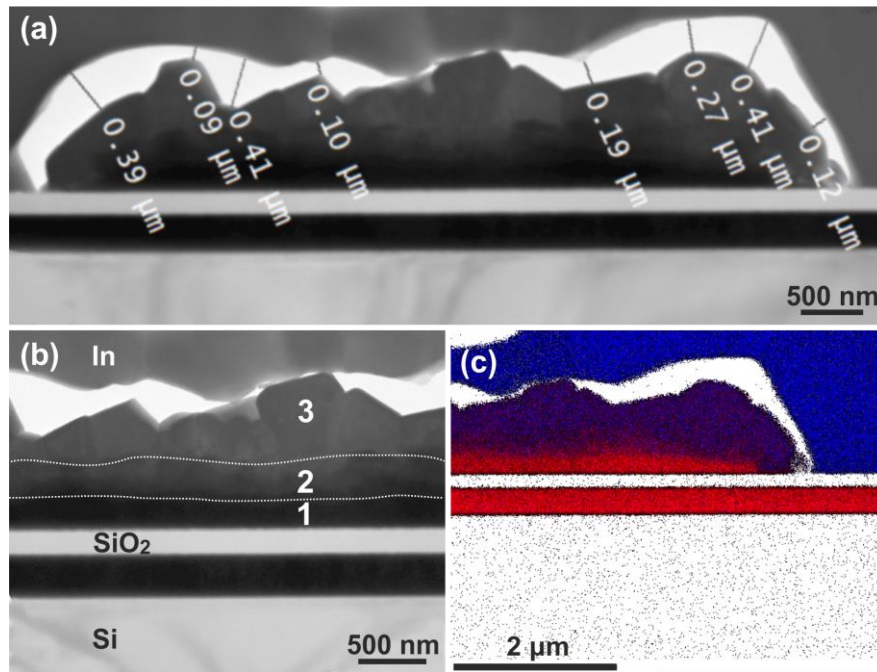


**Fig. 2.** Sample A: TEM cross-section of In column with voids (a), TEM image of the centre of the area visible in Fig. 2(a) (b), EDS map showing changes in Au/In concentration with distance from the UBM, red colour – Au, blue colour – In (c).

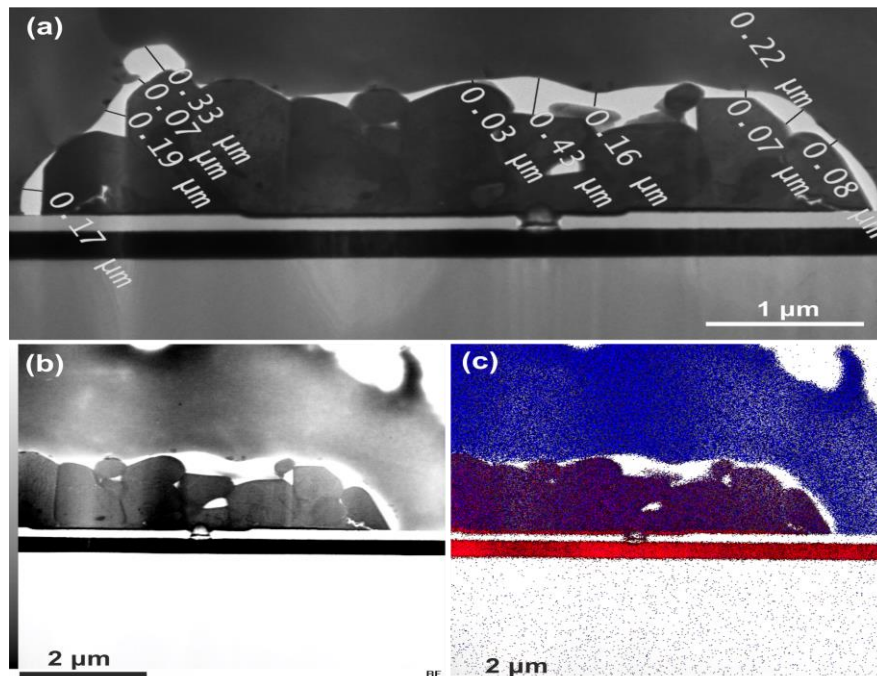


**Fig. 3.** Sample B: TEM cross-section of annealed In column with voids (a), TEM image of the right side of the area visible in Fig. 3(a) (b), the EDS map showing constant Au/In concentration ratio in the alloy volume, red colour – Au, blue colour – In (c).

The intermetallic alloy is 1.67 μm thick at its thickest point and has a uniform composition. It contains only column-shaped grains with a height of up to 1.67 μm and a width of up to 1.1 μm. The intermetallic alloy composition was verified similarly to sample A in a few cross-sectional points, in analogous areas marked in Fig. 2(b), starting from the area close to the SiO<sub>2</sub> layer. The composition values are similar in all measured points. The intermetallic alloy is uniform and contains 40% Au and 60% In. The material above the void is pure indium, while pure gold is

underneath the SiO<sub>2</sub> layer. The EDS map confirms the presence of pure In above the void, Au-In alloy with constant composition, and a very thin layer of pure Au near SiO<sub>2</sub> layer, as shown in Fig. 3(c).

The third sample (C) was prepared to clarify the issue of the voids between the intermetallic alloys and pure indium. The cross-section of annealed In columns was made with the cooled FIB stage. SEM images are shown in Fig. 4. Since no voids were observed, the preparation of cross-section for TEM measurements was abandoned. In Ref. 15,

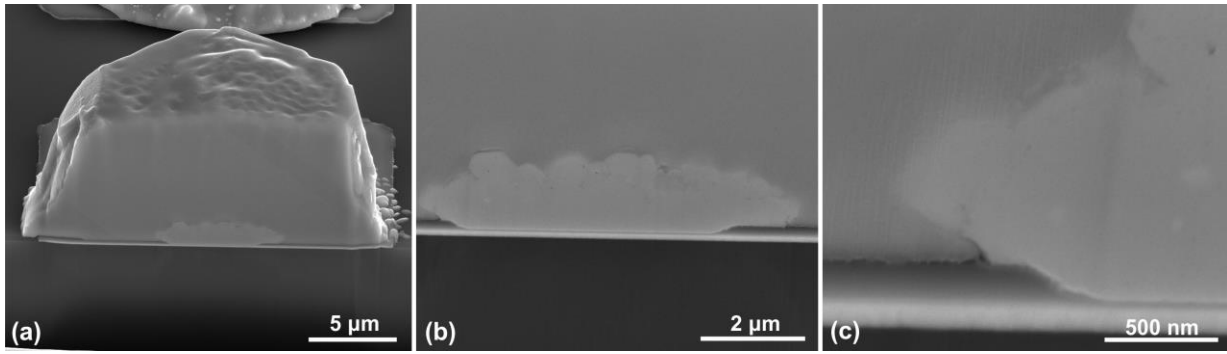


**Fig. 4.** Sample C: SEM images of In columns annealed at 120 °C during 5 min (a), FIB cross-section made with plate cooling (b), FIB cross-section under higher magnification (c).

the authors observed similar gaps and concluded that the lack of cooling during the FIB preparation was the reason for sample degradation at the Au-In alloy and pure indium material interface.

#### 4. Discussion

The intermetallic alloy in non-annealed In columns is 1.21  $\mu\text{m}$  thick (in the thickest point), including a layer of pure gold underneath. The estimated thickness of the Au layer is about 190 nm, whereas the starting thickness was 300 nm. The remaining Au layer did not participate in the process of forming the intermetallic alloy. This means that Au atoms migrated about 1.1  $\mu\text{m}$  from the 110 nm thick Au layer within 3 h at room temperature (RT) from the start of the indium deposition. The intermetallic alloy has a graded composition starting from pure gold and terminating with Au-In alloy with a composition ratio of 40–60%. The yield of non-annealed In columns changed in time: from 50–60% the day of their deposition to 70–80% after a few months, kept at RT. The In columns fell off in 1M HCl, leaving a grey circular field shown in Fig. 5(a). The colour of the material left over from the columns (observation under an optical microscope) indicates that it is an alloy rather than gold. TEM investigations revealed that the remaining material is a textured intermetallic alloy with a graded composition. Four areas were extracted from the TEM cross-section presented in Fig. 5(b). The first one is represented by a solid black zone located close to the SiO<sub>2</sub> layer. Three others with grains of different dimensions are shown as dark grey, light grey, and white (with texture) areas. It was observed that the brighter the area, the bigger the grains are. These areas differed in chemical composition.

The quantitative data are presented in Table 1. As can be seen, the chemical composition is constant within the selected area. Indium concentration increases from the bottom to the top up to about 63%. As a result, the composition of the Au-In alloy near and at the surface is on average 37–63%. It is close to the one obtained from the TEM-EDS cross-section of intermetallic alloy near the void (40–60%) for sample A. Similar composition (40–60%) was measured for the annealed column on sample B, where the yield was above 99%. This means that the differences in the chemical composition of the alloys were not the cause of the columns falling off. The origin of this problem can be found in other differences between samples, namely the thickness of inter-metallic alloy layers, their homogeneity, and grain sizes.

The thickness of the intermetallic alloy was 1.02  $\mu\text{m}$  (without the pure Au layer of 190 nm – sample A). Annealing of In columns at 120 °C increases the Au diffusion length and reduces the thickness of the pure Au layer, which, in the authors' case, ended up being almost zero. It means that the entire 300 nm thick Au layer was used to form the 1.67  $\mu\text{m}$  Au-In alloy. The thickness of the alloy for sample B is 50% higher (by 650 nm) as compared to sample A. Au atoms diffused up to about 1.37  $\mu\text{m}$  during the annealing (120 °C, 5 min), if we assume that the void indicates the border of Au-In alloy. The latter was formed at the interface between Au-In alloy and pure indium material by removing In grains as they have smaller hardness than the alloy (Mohs hardness is 1.2 and 2.5 for In and Au, respectively). In Ref. 4, the Au layer of a 4  $\mu\text{m}$  thickness was used to form a 1.6  $\mu\text{m}$  thick intermetallic layer during a 5 min long annealing. There was no information on whether it increased over time. In the

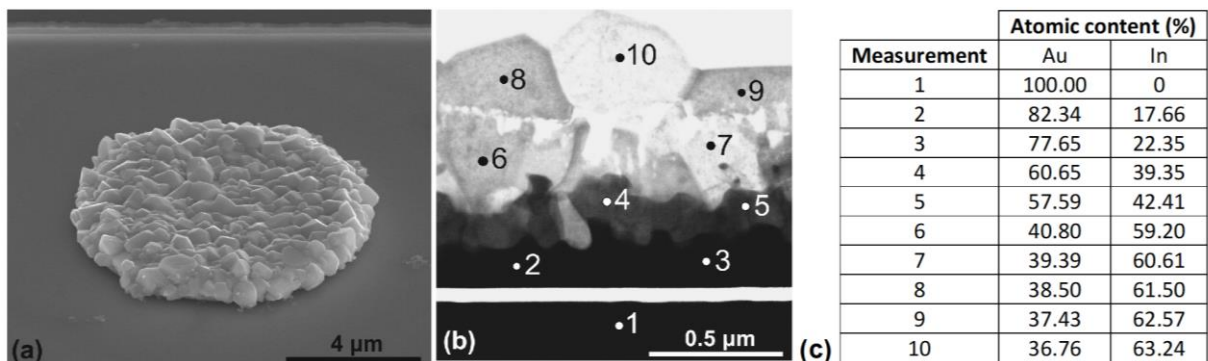


**Fig. 5.** Sample A: SEM image of the remnant of non-annealed In column (a), STEM-BF (bright field) image of In column remnant (b), TEM-EDS quantitative analysis of chemical composition across the In column remnant (c).

authors' case, the intermetallic alloy has comparable thickness, but it was formed from only an initial 0.3  $\mu\text{m}$  thick Au layer. The theoretical calculation presented in Ref. 16 shows that a unit volume of Au results in 4.2 unit volumes of AuIn<sub>2</sub>. A value of 5.6 was obtained for our experiment, which is 30% higher than the cited calculation. The non-uniformity of the intermetallic alloy, along with smaller grains, can also be considered as a potential cause of In columns falling off. The layered structure of Au-In alloy for sample A resulted in smaller grains as compared to sample B, where the column-shaped grains were formed during the coalescence process at elevated temperatures. The average grain size in sample A was twice smaller than for sample B. Assuming cubic geometry, this translates into an eight-fold increase in the number of grain boundaries and a twelve-fold increase in specific surface area, which enhances the etching rate along the grain boundaries due to their higher energy compared to the bulk, resulting in the In columns falling off. In other words, the improvement of yield to above 99% originates from a uniform Au-In alloy layer consisting of large grains in the shape of wide columns.

## 5. Conclusions

TEM cross-sections of In columns have been investigated to explain the difference between yields from fabrication processes with and without annealing. EDS analysis allows for distinguishing the chemical composition of intermetallic alloys in non-annealed and annealed In columns. The voids at the interface between intermetallic alloy and indium were identified to be caused by non-cooled FIB preparation. The gap appears probably due to the removal of In grains from the interface of Au-In and pure In layer by the ion beam. This gap allowed for the determination of the intermetallic alloy thickness. It was 1.02  $\mu\text{m}$  and 1.67  $\mu\text{m}$  for samples A (non-annealed) and B (annealed), respectively. In the case of sample A, the pure Au layer with a thickness of 190 nm did not participate in the formation of the intermetallic alloy, while for sample B the entire Au layer (300 nm) reacted with In. The Au-In inter-metallic alloy had a graded chemical composition ending with 40–60% at the surface and a constant composition of 40–60% for samples A and B, respectively. The surfaces of the remnants left after the In columns fell off were made of Au-In alloy containing 38% Au and 62% In. This proved that the chemical composition did not impact the yield. On the other hand, the intermetallic alloy thickness, its uniformity, and grain size can play a decisive role. The intermetallic alloy was layered and columnar for samples A and B, respectively. The grains were twice as big in the case of sample B. Thus, an intermetallic alloy thickness of 1.67  $\mu\text{m}$  and a uniform structure containing column-shaped grains with a base diameter of about 1.0  $\mu\text{m}$  were decisive factors in the improvement of yield to above 99%.

## Authors' statement

Research concept and design, P.K. and A.J.; collection and/or assembly of data, A.Ł.; data analysis and interpretation, P.K. and K.C.; writing the article, P.K., A.J. and K.C.; critical revision of the article, A.J. and K.Ch.; final approval of article, A.J. and K.Z.

## Acknowledgements

The research was carried out as part of the "Implementation Doctorate" program of the Ministry of Education and Science in Poland, project No. DWD/6/0329/2022, and partially funded by the National Center for Research and Development (NCRD) from projects POIR.04.01.04-00-0123/17-00.

## References

- [1] Huang, Y. Lin, C. Ye, Z.-H. & Ding, R.-J. Reflow flip-chip bonding technology for infrared detectors. *J. Micromech. Microeng.* **25**, 085009 (2015). <https://doi.org/10.1088/0960-1317/25/8/085009>
- [2] Walther, M. et al. Growth of InAs/GaSb short-period superlattices for high-resolution mid-wavelength infrared focal plane array detectors. *J. Cryst. Growth* **278**, 156–161 (2005). <https://doi.org/10.1016/j.jcrysgro.2004.12.044>
- [3] Breibach, J., Lübelsmeyer, K., Masing, T. & Rente, C. Development of a bump bonding interconnect technology for GaAs pixel detectors. *Nucl. Instrum. Methods Phys. Res. A* **470**, 576–582 (2001). [https://doi.org/10.1016/S0168-9002\(01\)00785-9](https://doi.org/10.1016/S0168-9002(01)00785-9)
- [4] Huang, Q., Xu, G., Yuan, Y., Cheng, X. & Luo, L. Development of indium bumping technology through AZ9260 resist electroplating. *J. Micromech. Microeng.* **20**, 055035 (2010). <https://doi.org/10.1088/0960-1317/20/5/055035>
- [5] Sjödin, S. A. Indium bump fabrication using electroplating for flip chip bonding. (Mid Sweden University, 2016).
- [6] Chu, K.-M., Lee, J.-S., Cho, H.-S., Park, H.-H. & Jeon, D.-Y. A Fluxless Flip-Chip Bonding for VCSEL Arrays Using Silver-Coated Indium Solder Bumps. in *2004 International IEEE Conference on the Asian Green Electronics (AGEC)* 246–253 (IEEE, 2004). <https://doi.org/10.1109/TEPM.2004.843155>
- [7] Kanazawa, S. et al. 214-Gb/s 4-PAM operation of flip-chip interconnection EADFB laser module. *J. Light. Technol.* **35**, 418–422 (2017). <https://doi.org/10.1109/JLT.2016.2632164>
- [8] Bah, M. A. et al. Indium bump deposition for flip-chip micro-array image sensing and display applications. *Proc. SPIE* **10639**, 1063921 (2018). <https://doi.org/10.1117/12.2303735>
- [9] Long, J. P., Varadaraajan, S., Matthews, J., Schetzina, J. F. & Schetzina, J. F. UV detectors and focal plane array imagers based on AlGaIn p-i-n photodiodes. *Opto-Electron. Rev.* **10**, 251–260 (2002). [https://optor.wat.edu.pl/10\(4\)251.pdf](https://optor.wat.edu.pl/10(4)251.pdf)
- [10] Tomada, A. et al. Flip Chip Assembly of Thin Substrates, Fine Bump Pitch, And Small Prototype Die. *Slack-Pub16168 (SLAC National Accelerator Laboratory)*. (2014). <https://www.slac.stanford.edu/pubs/slacpubs/16000/slac-pub-16168.pdf>
- [11] Jiang, J., Tsao, S., O'Sullivan, T., Razeghi, M. & Brown, G. J. Fabrication of indium bumps for hybrid infrared focal plane array applications. *Infrared Phys. Technol.* **45**, 143–151 (2004). <https://doi.org/10.1016/j.infrared.2003.08.002>
- [12] Broennimann, C. et al. Development of an Indium bump bond process for silicon pixel detectors at PSI. *Nucl. Instrum. Methods Phys. Res. A* **565**, 303–308 (2006). <https://doi.org/10.1016/j.nima.2006.05.011>
- [13] Lian, J., Jan, S., Chun, W., Goorsky, M. S. & Wang, J. Mechanical behavior of Au-In intermetallics for low temperature solder diffusion bonding. *J. Mater. Sci.* **44**, 6155–6161 (2009). <https://doi.org/10.1007/s10853-009-3851-7>
- [14] Kozłowski, P. et al. Indium-based micro-bump array fabrication technology with added pre-reflow wet etching and annealing. *Materials* **14**, 6269 (2021). <https://doi.org/10.3390/ma14216269>
- [15] Dantas de Moraes, L., Chevalliez, S. & Moulères, L. Low temperature FIB cross section: Application to indium micro bumps. *Microelectron. Reliab.* **54**, 1802–1805 (2014). <https://doi.org/10.1016/j.microrel.2014.08.004>
- [16] Siekhaus, W. J. et al. *Reaction of Gold with Indium Below 50°C: Radius Loss Delta R and Standard Deviation Sigma of Soldered 4 mil Wires at 100 Years Predicted from Measured Delta R and Sigma at 30 Years*. US Department of Energy, LLNL-TR-637432 (2013). <https://www.osti.gov/servlets/purl/1084699>